

RSC Advances



This is an *Accepted Manuscript*, which has been through the Royal Society of Chemistry peer review process and has been accepted for publication.

Accepted Manuscripts are published online shortly after acceptance, before technical editing, formatting and proof reading. Using this free service, authors can make their results available to the community, in citable form, before we publish the edited article. This *Accepted Manuscript* will be replaced by the edited, formatted and paginated article as soon as this is available.

You can find more information about *Accepted Manuscripts* in the [Information for Authors](#).

Please note that technical editing may introduce minor changes to the text and/or graphics, which may alter content. The journal's standard [Terms & Conditions](#) and the [Ethical guidelines](#) still apply. In no event shall the Royal Society of Chemistry be held responsible for any errors or omissions in this *Accepted Manuscript* or any consequences arising from the use of any information it contains.

Cite this: DOI: 10.1039/c0xx00000x

www.rsc.org/xxxxxx

ARTICLE TYPE

Enhancing Catalytic Activity and Stability for CO₂ Methanation on Ni-Ru/ γ -Al₂O₃ via Modulating Impregnation Sequence and Controlling Surface Active Species

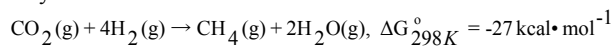
Wenlong Zhen ^{a,b}, Bo Li ^{a,b}, Gongxuan Lu ^{b,*}, Jiantai Ma ^a

⁵ Received (in XXX, XXX) Xth XXXXXXXXX 20XX, Accepted Xth XXXXXXXXX 20XX
DOI: 10.1039/b000000x

Bimetallic Ni-Ru NPs loaded onto γ -Al₂O₃ were prepared by co-impregnation and sequential impregnation methods and were investigated for CO₂ methanation in the temperature range of 250–500°C under atmospheric pressure to uncover the dependence of activities on surface species. It was found that the activities of CO₂ methanation were dependent on preparation sequence very significantly. Compared activity results dependence with the characterization results of XRD, H₂-TPR, BET, TEM-EDX and XPS techniques, it was indicated that the dispersion of Ru and Ni was controlled by preparation steps, and the tendency of Ru segregation on the catalyst surface was identified. This tendency led to the high activity of 10Ni-1.0Ru catalyst. Such surface segregation phenomenon of Ru in co-impregnation process controlled the chemical state of surface Ru species, made it to be easily reduced to metallic state. In addition, the 10Ni-1.0Ru catalyst performed with high stability and showed almost no deactivation up to 100h long term stability test. The possible reaction mechanism was proposed, in which CO₂ was dissociation and was activated on Ru species surface to form carbon species (CO_{ads}), and then was reacted with activated H on Ni centre to form methane.

20 Introduction

It is well known that the increase of carbon dioxide concentration in the atmosphere has resulted in remarkable climate change.¹⁻⁴ At present, CO₂ capture and storage (CCS) is considered as a main large scale method to solve CO₂ problem.⁵⁻⁸ For its chemical utilization, CO₂ can be converted into many chemicals, such as synthesized urea, salicylic acid, methanol, DME and DMC, aliphatic polycarbonate, CH₄, low carbon hydrocarbon. One main handicap in CO₂ chemical conversion is its high stability and inertness properties. Previous papers indicated that CO₂ can be converted into CH₄ in the presence of an adequate catalyst.⁹⁻¹³



This reaction is called the Sabatier reaction, operating temperatures at 400°C.¹⁴

A number of catalysts were reported to be active for Sabatier reaction, such as supported VIII metals and noble metals (e.g., Ru, Rh) on oxide supports. Among those catalysts, Ni-based catalyst was the most extensively studied, for example, Ni/MCM-41, Ni-La/ γ -Al₂O₃, Ni/RHA-Al₂O₃, Ni/ZrO₂-Al₂O₃ catalysts exhibited high activities at low temperature.¹⁵⁻²¹ Small Ni crystals in highly dispersed state on the catalyst surface might play an important role. One problem of Ni-based catalysts is its deactivation due to the interaction of the metal particles with carbon monoxide and formation of mobile nickel sub carbonyls.²² Noble metals such as Ru or Rh exhibited good resistant properties to sintering and carbon deposition than Ni,²³⁻²⁵ and showed high

activity and stability.^{7, 10, 22, 26-30} Therefore, Ni-Ru bi-metal catalyst has attracted extensive attention.³¹⁻³² The Ni-Ru bimetallic clusters on silica caused a strong improvement in the activity and stability of this bimetallic system.³³ It is known that the Ru dispersion and its chemical state on the support may play a key role in its catalytic performance,³⁴⁻³⁵ which means the control of surface species in catalyst preparation is needed for further understanding.

In this work, two methods, co-impregnation and sequential impregnation, were used to prepare a series of Ni-Ru/ γ -Al₂O₃ catalysts. By comparison the structure, surface species and catalytic performances of different catalyst, we uncovered the surface species segregation of Ru in Ni-Ru catalysts.³⁶ This effect of segregation on catalytic properties was also discussed, and the possible reaction mechanism for CO₂ methanation was proposed.

Experimental

Preparation of the catalysts

A series of Ni-Ru bimetallic catalysts were prepared by co-impregnation and sequential impregnation methods using Ni(NO₃)₂·6H₂O (AR, Shanghai NO.2 Reagent Co. Ltd.) and RuCl₃·xH₂O (AR, Shanghai Shanpu Chem. Corp., Ltd.) as a precursor. The nickel loading was 10wt% and ruthenium loading is 0.5, 1.0, 2.5, and 5.0% on γ -Al₂O₃ (40 mesh, Shanghai Meyer Chemical Technology Co., Ltd.). Before impregnation, the support γ -Al₂O₃ was stabilized in air at 600°C for 6h. After impregnation, the catalyst precursor was dried at room

temperature for 24h and at 110°C for another 24h. Finally, the precursor was calcined at 450°C for 5h. Here, the 10Ni-xRu/ γ -Al₂O₃ catalysts were prepared by co-impregnation method, which was denoted as 10Ni-xRu. In sequential impregnation process, the catalyst that the first step impregnated Ni and the final step impregnated Ru was denoted as 10Ni-1.0Ru(F), otherwise, it was denoted as 10Ni(F)-1.0Ru.

Catalytic activity

A reductive pre-treatment was performed before test.³⁷⁻³⁸ 100mg of the catalyst was loaded in each run and diluted with equal amount of quartz. The calcined catalysts were pre-reduced in-situ in a 60% H₂/N₂ stream for 2h with a total gas flow of 70mL·min⁻¹ at 450°C with a heating ramp of 10°C·min⁻¹.

Catalytic performances tests were conducted at atmospheric pressure in a fixed-bed continuous flow quartz reactor in the temperature range from 250 to 500°C. A K-type thermocouple was inserted in the furnace to measure the pre-treatment and reaction temperature. The reactor was heated in a tube furnace equipped with a temperature controller. All gases were monitored by calibrated mass flow controllers.

The H₂ and CO₂ reactants were mixed at a H₂:CO₂ ratio of 4:1 and N₂ was added as a carrier gas and internal standard for gas analysis. They were introduced into the reactor at a molar ratio of H₂:CO₂:N₂=4:1:4 and the total flow rate were set to 90 mL·min⁻¹.

The gas hourly space velocity (GHSV) was varied between 3000 and 15000h⁻¹. GHSV was varied by changing the catalyst mass while keeping the reactant flows constant. The gas phase products were analyzed on two on-line chromatographs equipped with thermal-conductivity detectors (TCD). Hydrocarbons as well as oxygenated products were separated with a GC112A (SDPTOP, Shanghai in China; column: HP-5, 30m×0.53mm×0.5μm) and analyzed by means of a flame ionization detector (FID). The detection limit for the products was 1×10⁻²vol. % at the given conditions. CO₂ conversion, CH₄ yield, CH₄ and CO selectivity were defined as follows:

$$X_{\text{CO}_2}(\%) = \left(1 - \frac{\text{CO}_2 \times (\text{N}_2)_{\text{in}}}{\text{N}_2 \times (\text{CO}_2)_{\text{in}}}\right) \times 100$$

$$S_{\text{CH}_4}(\%) = \frac{\text{CH}_4}{\text{CO}_2 + \text{CH}_4 + \text{CO} + 2\text{C}_2\text{H}_6} \times 100$$

$$S_{\text{CO}}(\%) = \frac{\text{CO}}{\text{CO}_2 + \text{CH}_4 + \text{CO} + 2\text{C}_2\text{H}_6} \times 100$$

Where X is the conversion, S is the selectivity, P and (P)_{in} are the reactant/product molar quantities at the exit and at the entrance of the reactor, respectively.

Characterization of the catalysts

Temperature-programmed reduction analysis (H₂-TPR) was carried out by heating a sample (50mg) from 25 to 700°C at 10°C min⁻¹ in a flow of 5 vol% H₂/Ar mixture (40 mL min⁻¹). The amount of H₂ consumed was measured by a TCD.

The X-ray diffraction patterns (XRD) of the samples were recorded on a Rigaku B/Max-RB X-ray diffractometer with a nickel-filtrated Cu K α radiation over a 2 θ range of 15-85° and a position sensitive detector using a step size of 0.017° and a step time of 15s at 40 mA and 40 kV.

X-ray photoelectron spectroscopy (XPS) analysis was performed using a VG Scientific ESCALAB 250Xi-XPS photoelectron spectrometer with an Al K α X-ray resource. The binding energies were calibrated by the C1s binding energy of 284.7 eV.

The specific surface areas (SSA) of the catalysts were determined by N₂ adsorption-desorption measurements at 77 K by employing the Brunauer-Emmet-Teller (BET) method (Micromeritics apparatus ASAP 2020M).

Transmission electron microscopy (TEM) and HRTEM images were taken with a Tecnai-G2-F30 field emission transmission electron microscope operating at accelerating voltage of 300 kV.

Results and discussion

Effect of temperature and preparation method on catalytic activity

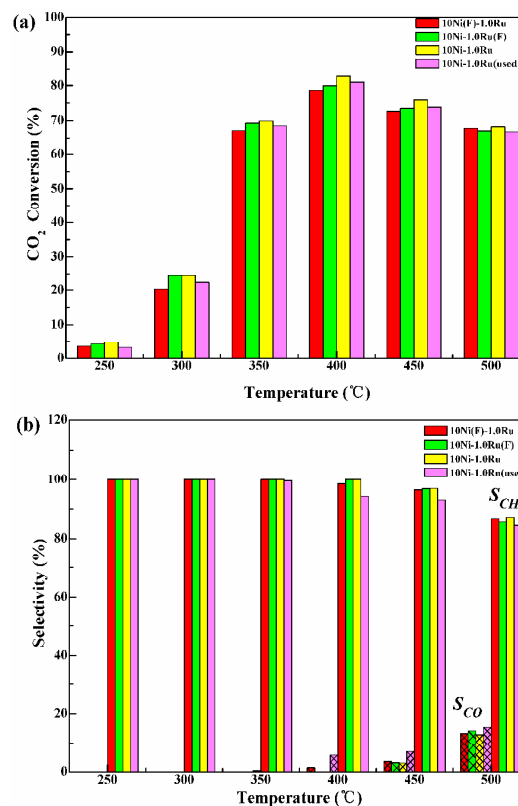


Fig. 1 Effect of temperature on the CO₂ conversion (a) and the CH₄ and CO selectivity (b) at the methanation of CO₂ over the 10Ni-1.0Ru, 10Ni-1.0Ru(F), 10Ni(F)-1.0Ru and 10Ni-1.0Ru(used) catalysts; Reaction conditions: 100 mg catalysts, H₂:CO₂=4:1, GHSV=9000h⁻¹, 1atm.

In order to investigate the influence of active species and effective active sites on catalytic performance, the 10Ni-1.0Ru, 10Ni(F)-1.0Ru, 10Ni-1.0Ru(F) and 10Ni-1.0Ru(used, after long-term reaction) catalysts were selected as the representatives and results were exhibited in Fig. 1. Fig. 1a showed that the CO₂ conversion increased with the reaction temperature increase (from 250 to 400°C), and followed by the gradual decrease (above 400°C) over all the samples. Fig. 1b showed the selectivity of CH₄ and by-product (CO) at the different reaction temperatures over all the samples. It was found that CH₄ selectivity was 100% below 400°C. CO was produced only above 400°C. Among 10Ni-1.0Ru, 10Ni-1.0Ru(F) and 10Ni(F)-1.0Ru, the 10Ni-1.0Ru

catalytic activity was higher (CO₂ conversion was 82.7%, the CH₄ selectivity was 100%) at 400°C, suggesting that more effective Ni and Ru species could be located on the surface of 10Ni-1.0Ru catalyst. The surface free energy of Ru was 3.05 J·m⁻², Ni was 2.45 J·m⁻², therefore, part of Ru atoms had been moved onto surface layer during co-impregnation,³⁹ which led to surface segregation. As a result, more effective Ni and Ru species could be located on the surface of 10Ni-1.0Ru catalyst. For 10Ni-1.0Ru(used), the catalytic activity was lower than other samples. This was possibly due to the change of active species on the surface of 10Ni-1.0Ru(used) during the long-term reaction.

XRD analysis

The crystal structures of the fresh and used catalysts were characterized by XRD method, the results were given in Fig. 2. The diffraction patterns of the 10Ni-1.0Ru, 10Ni (F)-1.0Ru, 10Ni-1.0Ru (F) and 10Ni-1.0Ru (used) catalysts showed similar typical peaks. The peaks at 44.5, 51.7, and 76.3° were the characteristic peaks of metallic Ni with a face-centered cubic structure (JCPDS# 87-0712). The peaks at 39.2, 42.3, and 44.0° could be assigned to the diffraction peaks of Ru with a hexagonal close-packed structure (JCPDS# 70-0274), while the peaks at 37 and 67° were assigned to the diffraction of γ -Al₂O₃ phase. The other weak diffraction peaks at 32° and 61° were also detected, which were the characteristic peaks of NiAl₂O₄.

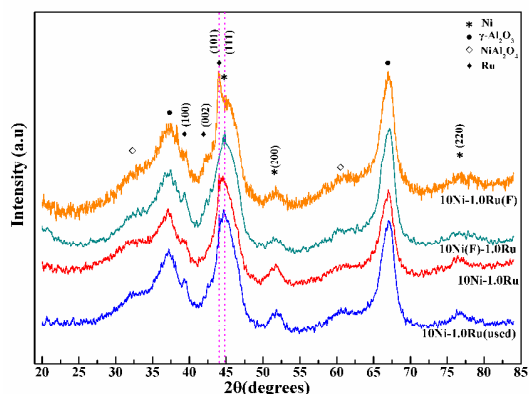


Fig. 2 XRD patterns of the 10Ni-1.0Ru, 10Ni-1.0Ru(F), 10Ni(F)-1.0Ru and 10Ni-1.0Ru(used) catalysts

In Fig. 2, the similar intensities of peaks assigned to (100), (200) and (220) facets of Ni implied that the preparation methods had no significant influence on the distribution of Ni species. However, the intensity of the peak at 44.0° assigned to the (101) facet of 10Ni-1.0Ru (F) sample was weaker compared with 10Ni-1.0Ru. The difference of surface Ru species among 10Ni-1.0Ru, 10Ni-1.0Ru (F) and 10Ni(F)-1.0Ru was resulted from the different impregnation sequences. In addition, the peaks of spinel (NiAl₂O₄) phase were observed, which was originated from the calcination of the nickel species located in the cationic deficient sites of alumina.⁴⁰ For 10Ni-1.0Ru catalyst, there was no significant difference before and after reaction, suggesting that the 10Ni-1.0Ru catalyst was stable during the reaction process.

TEM analysis

In order to better understand the role of Ni and Ru in the catalyst, the TEM and HRTEM images of Ni and Ru impregnated γ -Al₂O₃ were taken (Fig. 3a-f). The particle sizes distribution was showed

in the Fig. 3a-c. It could be noticed that nickel and ruthenium particles were small and uniformly dispersed in the 10Ni-1.0Ru and 10Ni-1.0Ru(F) samples. However, the agglomerative phenomenon occurred on 10Ni(F)-1.0Ru catalyst. This reflected the difference of preparation and calcination process. The average size of Ni and Ru particles on 10Ni-1.0Ru was about 7~9nm (Fig. 3a). The d-spacing of adjacent fringe for Ni nanocrystals was 0.204 nm, that could be indexed to the (111) crystalline plane of face-centered cubic Ni lattice. The d-spacings of 0.209nm and 0.234nm could be indexed to as the (101) and (100) crystalline plane of hexagonal close-packed Ru lattice, respectively. For 10Ni-1.0Ru(F) and 10Ni(F)-1.0Ru, the average particle sizes were 5~8 and 6~10 nm, respectively (Fig. 3b-c). The d-spacings of Ni(111) and Ru(101) were also given in Fig. 3e-f, which suggested that crystalline features of Ni and Ru particles on 10Ni-1.0Ru(F) and 10Ni(F)-1.0Ru were similar to that on 10Ni-1.0Ru. This result was in accordance with those results of XRD characterization.

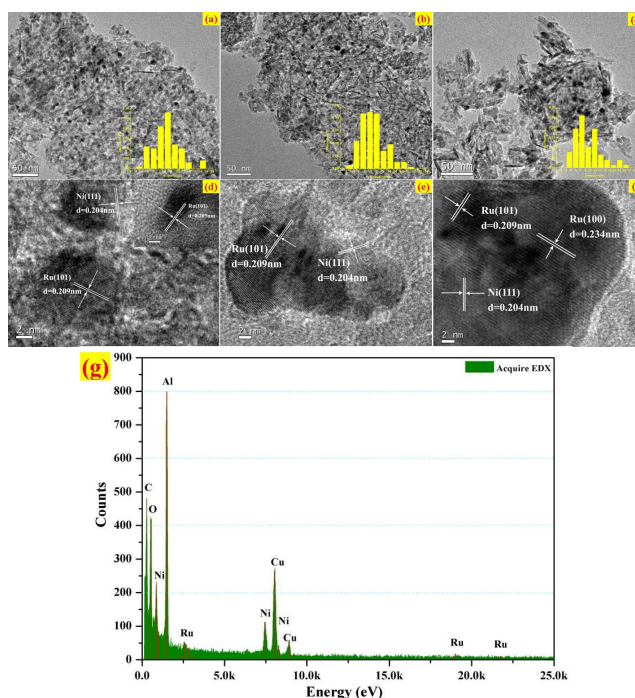


Fig. 3 TEM and HRTEM images of catalysts with different preparation methods: (a) and (d) 10Ni-1.0Ru; (b) and (e) 10Ni-1.0Ru (F); (c) and (f) 10Ni (F)-1.0Ru; (g) EDS spectrum of 10Ni-1.0Ru.

H₂-TPR analysis

H₂-TPR measurements were carried out to investigate the reducibility of the 10Ni-1.0Ru, 10Ni(F)-1.0Ru and 10Ni-1.0Ru(F) catalysts and the interaction between impregnated metal particles and supports. Fig. 4 showed TPR profiles of 10Ni-1.0Ru, 10Ni(F)-1.0Ru and 10Ni-1.0Ru(F) calcined at 450°C for 5h. All the catalysts showed two main reduction regions at 225 and 400°C. The reduction peaks of surface Ni species and Ru species were at 400 and 225°C, respectively. The shapes of Ru species reduction peak of 10Ni-1.0Ru and 10Ni-1.0Ru(F) catalysts were similar, suggesting that those Ru species were same. The results were in good agreement with the results of XRD characterization. The Ru species of 10Ni(F)-1.0Ru was different from those of 10Ni-1.0Ru and 10Ni-1.0Ru(F). The

difference in the Ru species was one of the main influencing factors on the different catalytic activities. The shapes or intensities of Ni species reduction peak were very similar for the three catalysts mentioned above, implying that the surface Ni species of all the catalysts was almost same. Compared 10Ni-1.0Ru(used) with 10Ni-1.0Ru, it was found that the Ru species changed during the long-time reaction.

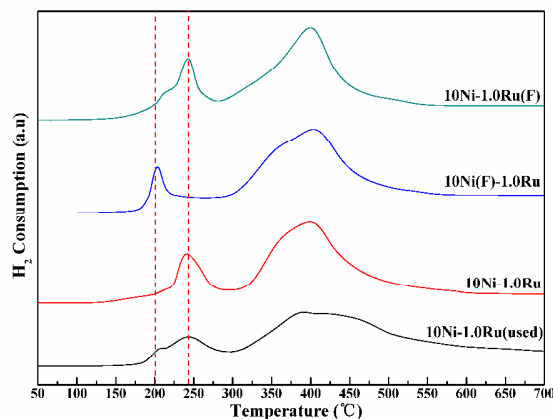


Fig. 4 H₂-TPR profiles of the 10Ni-1.0Ru, 10Ni-1.0Ru(F), 10Ni(F)-1.0Ru and 10Ni-1.0Ru(used) catalysts calcined at 450°C 5h.

BET

As shown in Fig. 5a, the nitrogen adsorption-desorption isotherms of all samples exhibited the IV type with H3 type hysteresis loop. The corresponding pore size distributions were very narrow at 10.0 nm (Fig. 5b), indicating the presence of mesopore structure in all the catalysts.

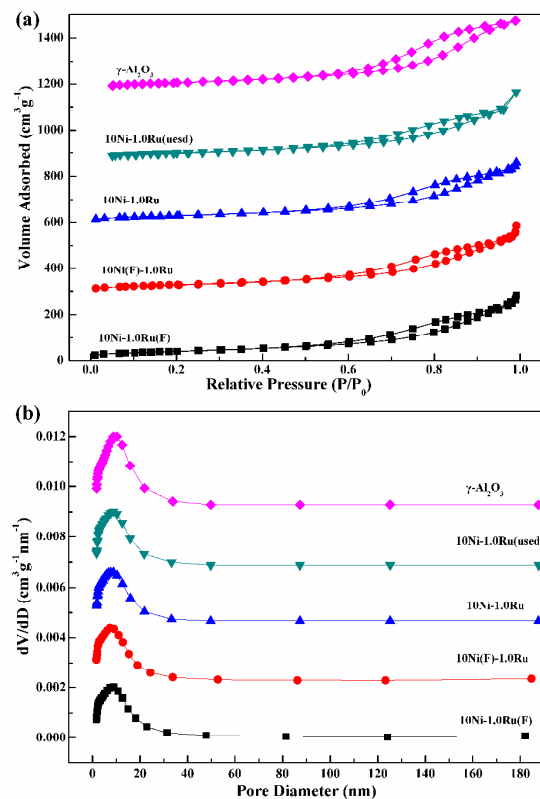


Fig. 5 Isotherms (a) and pore size distributions (b).

Table 1 Structural parameters obtained from N₂ adsorption isotherms analysis

Samples	S_{BET} (m^2g^{-1}) ^a	Pore volume (cm^3g^{-1}) ^b	Average pore size(nm) ^c
$\gamma\text{-Al}_2\text{O}_3$	169.6	0.4876	11.50
10Ni-1.0Ru(used)	149.0	0.4049	11.45
10Ni-1.0Ru	149.5	0.4736	12.67
10Ni(F)-1.0Ru	144.3	0.3759	9.941
10Ni-1.0Ru(F)	148.5	0.3699	10.27

^a Obtained from BET method

^b Total pore volume taken from the nitrogen adsorption volume at a relative pressure (P/P_0) of 0.99.

^c Average pore diameter determined from the adsorption data of the isotherms using BJH method.

The Brunauer-Emmett-Teller specific surface areas (S_{BET}) were determined by N₂ isotherms at 77K (as shown in Table 1). The S_{BET} of 10Ni-1.0Ru, 10Ni-1.0Ru (used), 10Ni-1.0Ru(F), 10Ni(F)-1.0Ru and $\gamma\text{-Al}_2\text{O}_3$ were 149.5, 149.0, 148.5, 144.3 and 169.6, respectively. 10Ni-1.0Ru and 10Ni-1.0Ru(F) had larger S_{BET} than that of 10Ni(F)-1.0Ru. Meanwhile, 10Ni-1.0Ru had the biggest pore volume and average pore size among these three samples, which benefited gas molecules diffusing into the holes.

XPS analysis

Fig. 6a showed typical XPS survey (wide-scan) spectra of the 10Ni-1.0Ru (fresh and used), 10Ni-1.0Ru(F), and 10Ni(F)-1.0Ru. Obviously, C, O, Al, Ni, and Ru elements with comparable peak intensities were presented on the surfaces of all the samples, which were verified by EDS characterization (Fig.3g). Here, the XPS spectra of the Ni2p and Ru3d of the four catalysts were presented in Fig. 6b-e. For the Ni2p, it was observed that the binding energies at 852.5, 857.9, 869.9, and 876.7eV were assigned to Ni2p_{3/2} (Ni), Ni2p_{3/2} (NiAl₂O₄), Ni2p_{1/2} (Ni), and Ni2p_{1/2} (NiAl₂O₄), respectively. It implied that Ni species on surface were Ni⁰ (Ni) and Ni²⁺ (NiAl₂O₄), which was strongly verified by the results of XRD.

The Ru3d spectra of all the catalysts were shown in Fig. 6b-e. The peaks at 280.1 (Ru3d_{5/2}) and 284.2eV (Ru3d_{3/2}) were observed for 10Ni-1.0Ru (fresh), 10Ni-1.0Ru(F), and 10Ni(F)-1.0Ru, suggesting that metallic Ru was present on the surface. The peak at 281.0eV were only present for 10Ni-1.0Ru(F) and 10Ni(F)-1.0Ru, and the intensity was weak, indicating that a small part of Ru species was RuO₂ for 10Ni-1.0Ru(F) and 10Ni(F)-1.0Ru. The RuO₂ originated from the incompletely reduced catalysts after calcined at 450°C for 5h. For the 10Ni-1.0Ru (used) catalyst (Fig. 6e), the peaks assigned to RuO₂ were also observed, which might originate from the partial oxidation of the ruthenium surface. Simultaneously, the C1s peak at 284.7eV indicated there was contaminated carbon on the surface of all samples. These results verified that the active species (Ru) had changed on the surface of 10Ni-1.0Ru (used) after reaction. Combined with the results of catalytic activity experiments, the higher catalytic activity of 10Ni-1.0Ru might result from the Ru species (Ru⁰).

The catalyst prepared by the co-impregnation method exhibited

the good catalytic performance. Therefore, The details of Ru loading, $H_2:CO_2$ molar ratios, GHSV, and stability were discussed in the subsequent sections.

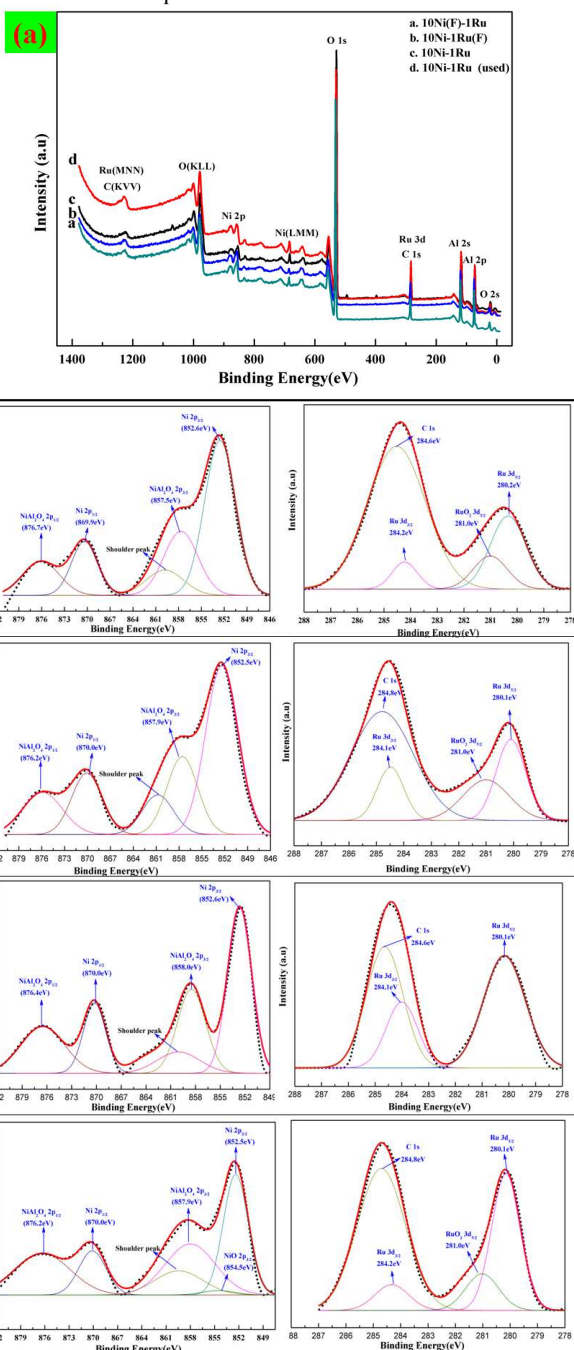


Fig. 6 All the samples XPS survey spectra (a); Ni 2p and Ru 3d XPS spectra for (b) 10Ni (F)-1.0Ru, (c) 10Ni-1.0Ru(F), (d) 10Ni-1.0Ru, and (e) 10Ni-1.0Ru (used).

Effect of Ru loading on catalytic activity

The catalytic activities of various 10Ni-xRu (x=0.5, 1.0, 2.5, and 5.0) catalysts prepared by co-impregnation method, with Ru loadings varying from 0.5 to 5.0 wt% were studied at temperatures ranging from 250 to 500 °C at a GHSV of 9000 h^{-1} , a $H_2:CO_2$ molar ratio of 4:1. The CO_2 conversion increased firstly with the reaction temperature increase from 250 to 400 °C, then

decreased (above 400 °C) (Fig. 7a). This might be due to the deactivation of the catalyst at higher temperature (above 400 °C). Fig. 7b showed the selectivity of CH_4 and CO. It was noticed that CO was the only by-product, which was produced on the surface of 10Ni-0.5Ru and 10Ni-5.0Ru catalysts above 350 °C. The CH_4 selectivity was always 100% from 250 to 350 °C for all samples, and was less than 100% for the 10Ni-1.0Ru and 10Ni-2.5Ru catalysts above 400 °C. Obviously, the conversion maximum was 82.71% for the 10Ni-1.0Ru at 400 °C. It was suggesting that 10Ni-1.0Ru might provide more active sites.

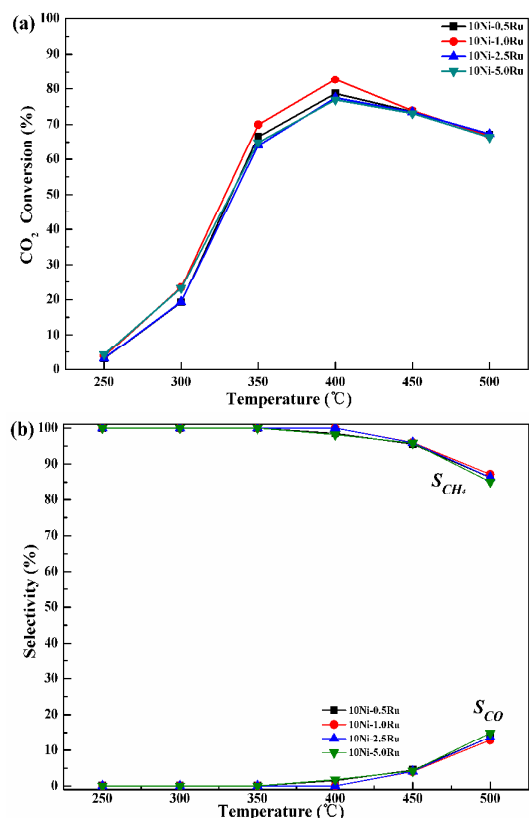


Fig. 7 Effect of temperature and Ru loading on the CO_2 conversion (a) and the selectivity (b) over 10Ni-xRu (x=0.5, 1.0, 2.5, 5.0) catalysts; Reaction conditions: 100 mg catalysts, $H_2:CO_2=4:1$, GHSV=9000 h^{-1} , 1 atm.

Effects of $H_2:CO_2$ molar ratio

Different $H_2:CO_2$ molar ratios were studied at a temperature ranging from 250 to 500 °C, GHSV was 9000 h^{-1} over the 10Ni-1.0Ru catalyst. CO_2 conversion and CH_4 selectivity over 10Ni-1.0Ru at different $H_2:CO_2$ molar ratios and temperatures were shown in Fig. 8.

CO_2 conversion and CH_4 selectivity increased when $H_2:CO_2$ molar ratios were increased from 2:1 to 6:1 at the same reaction temperature, but corresponding CO selectivity decreased. Fig. 8 showed that CO_2 conversion was 94.75% and CH_4 selectivity was 100% (at 400 °C, $H_2:CO_2$ molar ratio was 6:1). According to the results, it could be found that increasing $H_2:CO_2$ molar ratio was beneficial to CO_2 methanation.

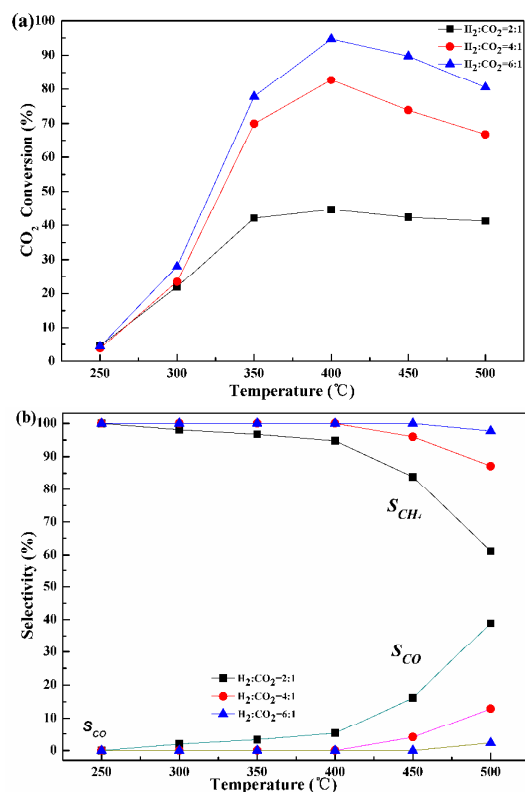


Fig. 8 The CO₂ conversion (a) and the selectivity (b) over 10Ni-1.0Ru catalyst at different H₂:CO₂ molar ratio (ranging from 2:1 to 6:1); Reaction conditions: 100 mg catalyst, GHSV=9000h⁻¹, 1atm.

Effects of GHSV

To study the effect of GHSV on the activity, the GHSV was varied between 3000 and 15000h⁻¹. Fig. 9 showed that the catalytic activity of 10Ni-1.0Ru was tested at different GHSV, H₂:CO₂ molar ratio was 4:1 and temperatures ranging from 250 to 500°C.

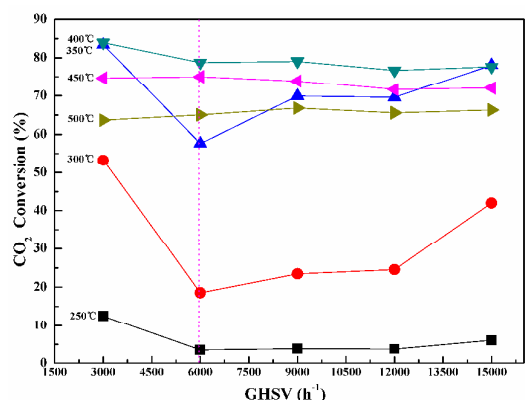


Fig. 9 The CO₂ conversion over 10Ni-1.0Ru catalyst at different GHSV (ranging from 3000 to 15 000 h⁻¹); Reaction conditions: 100 mg catalyst, H₂:CO₂=4:1, 1atm.

It was found that the temperature curves could be divided into two domains. First, CO₂ conversion decreased at GHSV between 3000 and 6000 h⁻¹. As the GHSV increased, the velocity for the reactants through the catalyst bed became larger; therefore, the contact time on the surface of the catalyst bed became shorter.

Thus, the thermodynamic equilibrium conversions for the reactants were not achieved due to insufficient contact time. In addition, the number of the reactants through the catalyst bed became larger with the increase of GHSV; consequently, the catalyst was not able to provide sufficient active sites for redundant reactants. In addition, CO₂ conversion almost remained constant at 400, 450 and 500°C when GHSV varied from 6000 to 15000h⁻¹, and the other three temperature curves (250, 300 and 350°C) showed a slow upward trend. In addition, regarding the mentioned-temperature curves, the optimum GHSV was 9000h⁻¹, meaning the entire catalyst works efficiently.

Long-term stability tests

Fig. 10 showed the catalytic activity during 100 h on CO₂ methanation over 10Ni-1.0Ru at 400°C and H₂:CO₂ molar ratio was 4:1, at 9000 h⁻¹. Obviously, CO₂ conversion remained above 82% and CH₄ selectivity was almost 100% during long-term over 10Ni-1.0Ru. The by-product (CO) was only produced on the 10Ni-1.0Ru catalyst after 80 hours. However, CO selectivity was less than 0.5%.

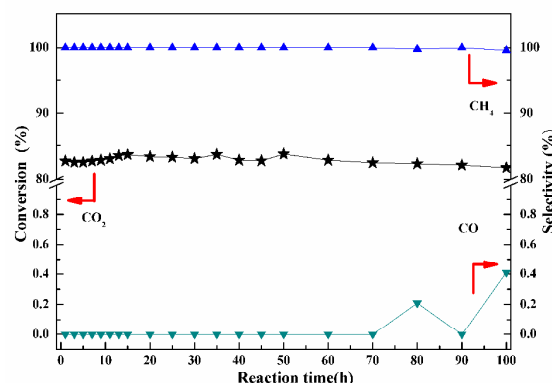


Fig. 10 Long-term (100h) stability tests over 10Ni-1.0Ru catalyst; Reaction conditions: 100 mg catalyst, H₂:CO₂=4:1, GHSV=9000h⁻¹, 1atm, 400°C

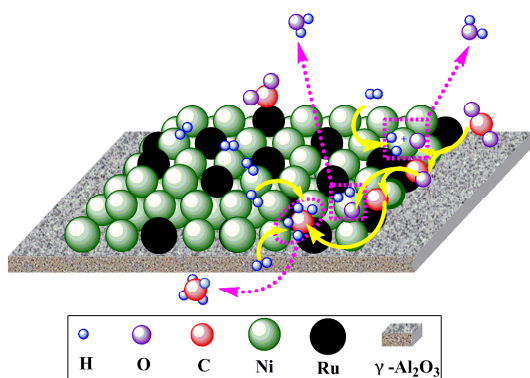
There were two reasons for the decrease of CH₄ selectivity after 80 hours. First of all, although the atmosphere was rather reductive in carbon dioxide methanation, the metallic nickel (Ni) of catalyst surface could be gradually re-oxidized to nickel oxide (NiO) by CO₂ or by water produced, deactivating the catalyst during the long-term reaction. The nickel species (Ni⁰ or Ni²⁺) located at the cationic deficient sites of γ -Al₂O₃ phase strongly interacted with the carrier, resulting in the formation of solid solution of nickel oxide (NiO) and nickel aluminate spinel phase (NiAl₂O₄) at 400°C^{39, 45-46}. The second reason was that the noble metal Ru was also oxidized to RuO₂. Noble metals (Ru, Pt, Rh, etc.) had better resistance to carbon deposition than Ni²³⁻²⁵, and enhanced the high activity and stability of the catalysts and achieved high CO₂ conversions with low carbon formation^{7, 10, 26-28}. The decrease of CH₄ selectivity was due to RuO₂ located on the surface of the catalyst. Therefore, all the phenomena mentioned above indicated that 10Ni-1.0Ru catalyst performed the excellent catalytic activity and stability.

Possible reaction mechanism of CO₂ methanation on 10Ni-1.0Ru

Scheme 1 gave a possible reaction mechanism of CO₂

methanation on 10Ni-1.0Ru. The methanation of CO₂ involved the conversion of CO₂ to CO prior to methanation, and the subsequent reaction followed the same mechanism as CO methanation.⁴⁷⁻⁴⁸

The first step of the methanation reaction could be the chemisorption of CO₂ on the catalyst and the dissociation of CO₂ into carbon species (CO_{ads}) and oxygen species (O_{ads}) on the surface.⁴⁹ At the same time, H₂ is dissociated into H on Ni. C. Crisafulli et al. studied H₂ adsorption on metallic Ni. Their work had emerged a picture of relatively facile H₂ dissociation on, and strong binding of atomic H to, most transition metals.⁴⁹⁻⁵⁰ The second step of carbon species (CO_{ads}) was dissociated into C and O on the surface of the catalysts. C could react with H to produce CH₄ on metallic Ru, and H and O atoms formed H₂O.⁵¹



Scheme 1 The proposed a possible reaction mechanism of CO₂ methanation over 10Ni-1.0Ru catalyst.

Conclusion

A series of bimetal Ni-Ru catalysts had been successfully prepared by co-impregnation and sequential impregnation methods. The obtained catalysts performed high catalytic activities, selectivities, and excellent stabilities for CO₂ methanation. Besides, it was also found that the segregation phenomenon of Ru occurred on the catalyst surface in the co-impregnation preparation process, by which more active Ni and Ru species (metallic Ru) could be provided on the surface of 10Ni-1.0Ru catalyst. The high catalytic activity was obtained at Ru loading of 1.0%, GHSV 9000h⁻¹ and higher H₂:CO₂ molar ratio. The 10Ni-1.0Ru showed more stable and highly active properties during the long-term reaction. Based on the characterizations, it was proposed that CO₂ was dissociated and activated to form carbon species (CO_{ads}) on Ru species surface, then reacted with activated H on Ni species to form methane.

Acknowledgment

This work is supported by the 973 and 863 Programs of the Department of Sciences and Technology of China (2013CB632404, 2012AA051501, 2009CB22003) and the NSF of China (grant no. 21173242), respectively.

Notes and references

- ^a State Key Laboratory of Applied Organic Chemistry, College of Chemistry and Chemical Engineering, Lanzhou University, Lanzhou, China. Tel.: +86 18298414700; E-mail: zhenwenlong123@126.com
^b State Key Laboratory for Oxo Synthesis and Selective Oxidation,

- Lanzhou Institute of Chemical Physics, Chinese Academy of Sciences, Lanzhou, China. Fax: +86 931 4968176; Tel: +86 931 4968176; E-mail: gxlu@lzb.ac.cn
- D. B. Dell'Amico, F. Calderazzo, L. Labella, F. Marchetti and G. Pampaloni, *Chemical Reviews*, 2003, **103**, 3857.
 - M. Mikkelsen, M. Jorgensen and F. C. Krebs, *Energy & Environmental Science*, 2010, **3**, 43.
 - W. WANG and J. L. Gong, *Frontiers of Chemical Science and Engineering*, 2011, **5**, 2.
 - Z. Y. Wang, H. C. Chou, J. Wu, D. P. Tsai and G. Mul, *Applied Catalysis A: General*, 2010, **380**, 172.
 - X. D. Xu and J. A. Moulijn, *Energy Fuels*, 1996, **10**, 305.
 - H. Yang, Z. Xu, M. Fan, R. Gupta, R. B. Slimane, A. E. Bland and I. Wright, *Journal of Environmental Sciences*, 2008, **20**, 14.
 - A. J. Hunt, E. H. K. Sin, R. Marriott and J. H. Clark, *ChemSusChem*, 2010, **3**, 306.
 - G. Ferey, C. Serre, T. Devic, G. Maurin, H. Jobic, P. L. Llewellyn, G. D. Weireld, A. Vimont, M. Daturi and J. S. Chang, *Chemical Society Reviews*, 2011, **40**, 550.
 - A. Beulsa, C. Swalusa, M. Jacquemina, G. Heyenb, A. Karellovica and P. Ruiza, *Applied Catalysis B: Environmental*, 2012, **113-114**, 2.
 - P. Sabatier and J. B. Senderens, *Comptes Rendus de l'Académie des Sciences*, 1902, **134**, 514.
 - A. D. Tomsett, T. Hagiwara, A. Miyamoto and T. Inui, *Applied catalysis*, 26 (1986) 391.
 - P. J. Lunde and F. L. Kester, *Industrial and Engineering Chemistry Process Design and Development*, 1974, **13**, 27.
 - K. R. Thampi, J. Kiwi and M. Graetzel, *Nature*, 1987, **327** 506.
 - K. P. Brooks, J. Hu, H. Zhu and R. J. Kee, *Chemical Engineering Science*, 2007, **62**, 1161.
 - G. D. Weatherbee and C. H. Bartholomew, *Journal of Catalysis*, 1981, **68**, 67.
 - D. E. Peebles, J. M. Goodman and J. M. White, *Journal of Physical Chemistry*, 1983, **87**, 4378.
 - M. Yamasaki, H. Habazaki, K. Asami, K. Izumiya and K. Hashimoto, *Catalysis Communications*, 2006, **7** 24.
 - G. Du, S. Lim, Y. Yang, C. Wang, L. Pfefferle and G. L. Haller, *Journal of Catalysis*, 2007, **249**, 370.
 - F. Guo, W. Chu, H. Xu and T. Zhang, *Chinese Journal of Catalysis*, 2007, **28**, 429.
 - M. Cai, J. Wen, W. Chu, X. Cheng and Z. Li, *Journal of Natural Gas Chemistry*, 2011, **20**, 318.
 - F. W. Chang, M. S. Kuo, M. T. Tsay and M.C. Hsieh, *Applied Catalysis A: General*, 2003, **247**, 309.
 - M. Agnelli, M. Kolb and C. Mirodatos, *Journal of Catalysis*, 1994, **148**, 9.
 - A. T. Ashcroft, A. K. Cheetham, M. L. H. Green and P. D. F. Vernon, *Nature*, 1991, **352**, 225.
 - P. D. F. Vernon, M. L. H. Green, A. K. Cheetham and A. T. Ashcroft, *Catalysis Today*, 1992, **13**, 417.
 - J. R. Rostrup-Nielsen and J. H. B. Hansen, *Journal of Catalysis*, 1993, **144**, 38.
 - J. R. Rostrup-Nielsen, *Catalysis Reviews: Science and Engineering*, 2004, **46**, 247.
 - E. Akpana, Y. Sun, P. Kumar, H. Ibrahim, A. Aboudheir and R. Idem, *Chemical Engineering Science*, 2007, **62**, 4012.
 - D. L. Trimm, *Catalysis Today*, 1999, **49**, 3.
 - A. L. Kustov, A. M. Frey, K. E. Larsen, T. Johannessen, J. K. Nørskov and C. H. Christensen, *Applied Catalysis A: General*, 2007, **320**, 98.
 - M. Ku śmierz, *Catalysis Today*, 2008, **137**, 429.
 - S. Hwang, J. Lee, U. G. Hong, J. H. Baik, D. J. Koh, H. Lim and I. K. Song, *Journal of Industrial and Engineering Chemistry*, 2013, **19**, 698.
 - D. J. Elliott and J. H. Lunsford, *Journal of Catalysis*, 1979, **57**, 11.
 - C. Crisafulli, S. Scirè, S. Minicò and L. Solarino, *Applied Catalysis A: General*, 2002, **225**, 1.
 - Z. Kowalczyk, K. Stolecki, W. Raróg-Pilecka, E. Miśkiewicz, E. Wilczkowska and Z. Karpiński, *Applied Catalysis A: General*, 2008, **342**, 35.
 - F. Solymosi, A. Erdohelyi and T. Banskagi, *Journal of Catalysis*, 1981, **68**, 371.

- 36 Y. Ni, W. Peng, A. Sun, W. Mo, J. Hu, T. Li and G. Li, *Journal of Industrial and Engineering Chemistry*, 2010, **16**, 503.
- 37 F. Ocampo, B. Louis and A. C. Roger, *Applied Catalysis A: General*, 2009, **369**, 90.
- 5 38 F. Ocampo, B. Louisa, L. Kiwi-Minskerb and A. C. Roger, *Applied Catalysis A: General*, 2011, **392**, 36.
- 39 H. L. Skriver and N. M. Rosengaard, *Physical Review B*, 1992, **46**, 7157.
- 40 A. Corma, V. Fornés, R. M. Martín-Aranda and F. Rey, *Journal of Catalysis*, 1992, **134**, 58.
- 10 41 J. Okal, M. Zawadzki and W. Tylus, *Applied Catalysis B: Environmental*, 2011, **101**, 548.
- 42 D. D. Sarma and C. N. R. Rao, *Journal of Electron Spectroscopy and Related Phenomena*, 1980, **20**, 25.
- 15 43 Y. C. Lin, C. Y. Lin and P. W. Chiu, *Applied Physics Letters*, 2010, **96**, 133110.
- 44 X. L. Cai, X. F. Dong and W. M. Lin, *Journal of Natural Gas Chemistry*, 2008, **17**, 98.
- 45 E. D. Dimotakis and T. J. Pinnavaia, *Inorganic Chemistry*, 1990, **29**, 2393.
- 20 46 J. A. Wang, X. Bokhimi, A. Morales and O. Novaro, *Journal of Physical Chemistry B*, 1999, **103**, 299.
- 47 J. L. Falconer and A. E. Zağli, *Journal of Catalysis*, 1980, **62**, 280.
- 48 M. Marwood, R. Doepfer and A. Renken, *Applied Catalysis A: General*, 1997, **151**, 223.
- 25 49 M. Jacquemin, A. Beuls and P. Ruiz, *Catalysis Today*, 2010, **157**, 462.
- 50 K. D. Rendulic, A. Winkler and H. P. Steinrück, *Surface Science*, 1987, **185**, 469.
- 51 P. D. Reed, C. M. Comrie and R. M. Lambert, *Surface Science*, 1976, 30 **59**, 33.

Graphical abstract

Enhancing Catalytic Activity and Stability for CO₂ Methanation on Ni-Ru/ γ -Al₂O₃ via Modulating Impregnation Sequence and Controlling Surface Active Species

In this work, two methods, co-impregnation and sequential impregnation, were used to prepare a series of Ni-Ru/ γ -Al₂O₃ catalysts. By comparison the structure, surface species and catalytic performances of different catalyst, we uncovered the surface species segregation of Ru in Ni-Ru catalysts. The effect of this segregation on catalytic properties was also discussed, and the possible reaction mechanism for CO₂ methanation was proposed.

